



RESEARCH LETTER

10.1002/2016GL069359

Key Points:

- Compressional end-glacial earthquakes in Fennoscandia occurred in a setting where the contemporaneous horizontal strain rate was extensional
- End-glacial earthquakes therefore tapped into tectonically derived strain accumulated and stored over a long timescale
- Seismic hazard in intraplate settings is influenced by nontectonic transients and may be more broadly distributed than commonly thought

Supporting Information:

- Supporting Information S1
- Figure S1
- Figure S2
- Figure S3
- Figure S4
- Figure S5
- Figure S6
- Figure S7
- Figure S8
- Figure S9

Correspondence to:

T. J. Craig,
t.j.craig@leeds.ac.uk

Citation:

Craig, T. J., E. Calais, L. Fleitout, L. Bollinger, and O. Scotti (2016), Evidence for the release of long-term tectonic strain stored in continental interiors through intraplate earthquakes, *Geophys. Res. Lett.*, 43, doi:10.1002/2016GL069359.

Received 27 APR 2016

Accepted 15 JUN 2016

Accepted article online 20 JUN 2016

Evidence for the release of long-term tectonic strain stored in continental interiors through intraplate earthquakes

T. J. Craig^{1,2}, E. Calais¹, L. Fleitout¹, L. Bollinger³, and O. Scotti⁴

¹Ecole normale supérieure, Department of Geosciences, PSL Research University, Paris, France, ²Institute of Geophysics and Tectonics, School of Earth and Environment, University of Leeds, Leeds, UK, ³CEA, DAM, DIF, Arpajon, France, ⁴IRSN/PRP-DGE/SCAN/BERSSIN, Fontenay-aux-Roses, France

Abstract The occurrence of large earthquakes in stable continental interiors challenges the applicability of the classical steady state “seismic cycle” model to such regions. Here we shed new light onto this issue using as a case study the cluster of large reverse faulting earthquakes that occurred in Fennoscandia at 11–9 ka, triggered by the removal of the ice load during the final phase of regional deglaciation. We show that these reverse-faulting earthquakes occurred at a time when the horizontal strain rate field was extensional, which implies that these events did not release horizontal strain that was building up at the time but compressional strain that had been accumulated and stored elastically in the lithosphere over timescales similar to or longer than a glacial cycle. We argue that the tectonically stable continental lithosphere can store elastic strain on long timescales, the release of which may be triggered by rapid, local transient stress changes caused by surface mass redistribution, resulting in the occurrence of intermittent intraplate earthquakes.

1. Introduction

The extent to which the classical concept of an observable and steady state “seismic cycle” applies to faults in stable continental interiors, with short-term observations of present-day strain rates through seismicity or geodesy being reliable proxies for seismic hazard, remains an open question [e.g., Newman *et al.*, 1999; Kenner and Segall, 2000; Smalley *et al.*, 2005; Calais and Stein, 2009; Stein and Liu, 2009; Hough and Page, 2011; England and Jackson, 2012; Page and Hough, 2014]. For some, faults in such settings are analogous to their plate boundary counterparts, although accumulating strain at very slow rates. Large earthquakes therefore repeat over time on individual faults as they do at plate boundaries, although with substantially longer recurrence intervals, and faulting is representative of a consistent and potentially observable strain rate field. This view is consistent with the interpretation of present-day intraplate seismic clusters as being indicative of focused areas of long-lived deformation [Page and Hough, 2014]. Alternatively, intraplate faults may be releasing strain stored in the elastic crust over long intervals but not necessarily localizing observable interseismic strain at their time of failure [Calais *et al.*, 2010]. Transient variations in crustal stress or fault strength, if large enough compared to the background tectonic stressing rates, may then trigger rupture. Because background tectonic loading in intraplate settings is very slow, rupture may not necessarily repeat on a given fault over timescales similar to, or longer than, a glacial cycle. This view is consistent with the clustering and migration of large intraplate earthquakes in space and time [Crone *et al.*, 2003; Liu *et al.*, 2010]. Given the slow rates of deformation, and limited observation period, both models have typically been heavily dependent on a relatively small number of type examples and case studies, largely focused on North America or eastern Asia [Crone and Luza, 1990; Smalley *et al.*, 2005; Stein and Liu, 2009; Liu *et al.*, 2010; Hough and Page, 2011; Craig and Calais, 2014; Page and Hough, 2014].

Here we use the seismicity of the Baltic Shield to shed new light onto this debate. Fennoscandia, a stable continental interior, evidences numerous large-scale fault scarps which developed during the early Holocene (11–9 ka) [Muir-Wood, 1989; Lagerbäck and Sundh, 2008] in an environment generally considered to be tectonically quiescent (Figure 1). The dimensions of these faults range from small-scale fractures to the 155 km long Pärvie fault scarp, with offsets exceeding 15 m in places [Lagerbäck, 1978; Muir-Wood, 1989; Lagerbäck and Sundh, 2008]. A number of these faults likely generated major earthquakes, with cumulative magnitudes exceeding M_w 8 on some of the faults [Muir-Wood, 1989; Arvidsson, 1996]—in stark contrast to the historical

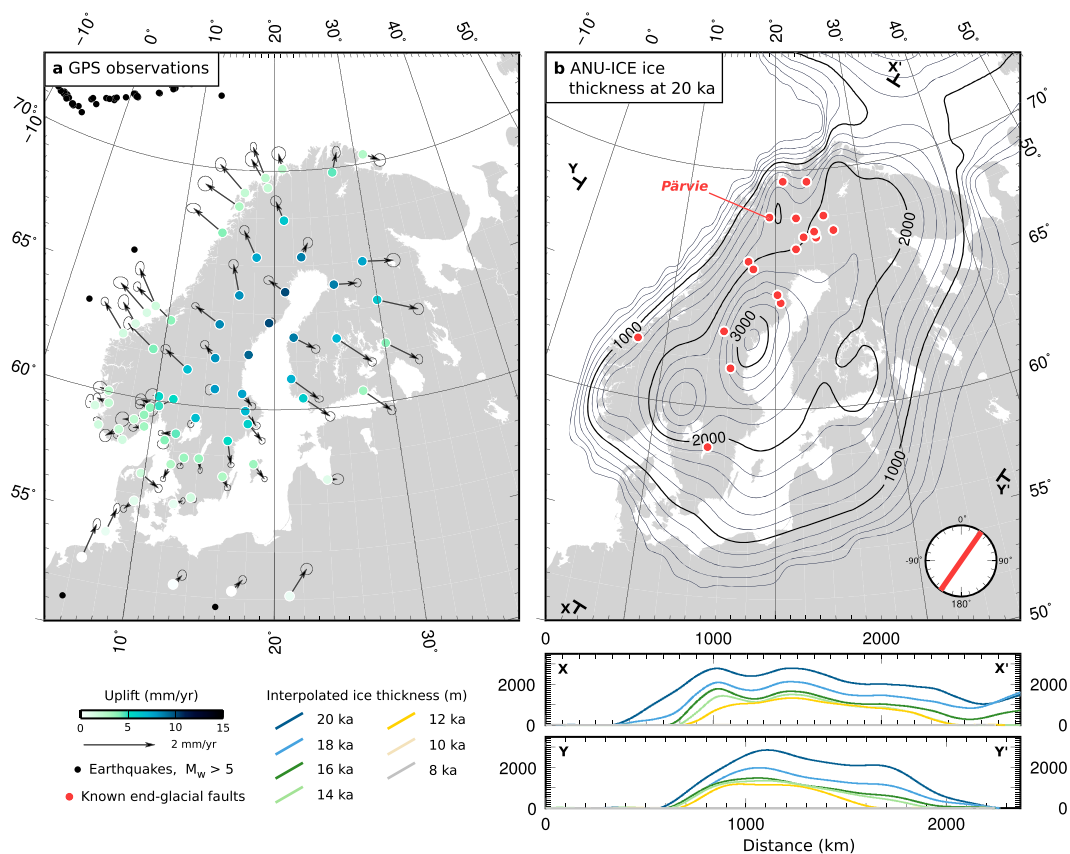


Figure 1. Influence of deglaciation on the deformation of Fennoscandia. (a) Present-day GPS observations across Fennoscandia [Kierulf *et al.*, 2014]. The colour of the circles indicates uplift rates. The reference frame used is fixed on the center of the GIA deformation pattern. Black dots show instrumentally recorded seismicity with $M_w > 5$ since 1977 (from <http://www.globalcmt.org>). (b) Interpolated ANU-ICE ice thickness at 20 ka. Red circles indicate the location of known end-glacial faults [Muir-Wood, 1989; Lagerbäck and Sundh, 2008; Jakobsen *et al.*, 2014; Olesen *et al.*, 2014; Smith *et al.*, 2014]. The compass rose in Figure 1b indicates the dominant strike of this population of faults. The profiles below Figure 1b show ice thicknesses along profiles XX' and YY' at 2 ka intervals between 20 ka and 8 ka (at which point, major deglaciation of the Fennoscandian Ice Sheet has ended). The location of the major Pärvie fault is indicated in Figure 1b.

and instrumental seismicity catalogues for Fennoscandia, which only rarely record events exceeding $M_w 5$ (see Figure 1a). These “end-glacial” faults are found in regions that were located beneath substantial ice thicknesses during the last glacial cycle (Figure 1b). Large-scale features are strongly concentrated in northern Sweden and Finland (the Lapland Fault Province), but distributed faulting is evidenced across much of Fennoscandia [Kotilainen and Hutri, 2004; Jakobsen *et al.*, 2014; Olesen *et al.*, 2014; Smith *et al.*, 2014]. Their clustering at 11–9 ka strongly suggests a link to the deglaciation [Muir-Wood, 1989; Lagerbäck and Sundh, 2008], a hypothesis consistent with mechanical modeling studies [Wu *et al.*, 1999; Wu and Johnston, 2000; Lambeck and Purcell, 2003; Turpeinen *et al.*, 2008; Lund *et al.*, 2009; Steffen *et al.*, 2014b], wherein the removal of the ice load leads to a concurrent peak in fault instability.

An apparent paradox surrounding these end-glacial earthquakes involves their sense of motion, as the majority are reverse faulting events [Muir-Wood, 1989] striking NNE-SSW and dipping at moderate-to-high angles ($\geq 35^\circ$) [Juhlin *et al.*, 2010], hence accommodating NW-SE compression. However, the present-day regional strain rate field (Figure 1a), dominated by postglacial rebound, indicates NW-SE extension across the length of Scandinavia, opposite to the sense of strain released by these major end-glacial ruptures. Long-term tectonic strain rates, unresolvable above the overprinting effect of postglacial rebound, are negligibly small [Kierulf *et al.*, 2014]. However, plate-scale geodynamic models suggest tectonic compression in a roughly NW-SE direction [Lund and Zoback, 1999; Heironymus *et al.*, 2008; Pascal *et al.*, 2010], consistent with the observed end-glacial faulting mechanism and with the overall orientation of small-scale instrumental seismicity [Slunga, 1991; Lindholm *et al.*, 2000].

Here we use postglacial rebound models to show that the large end-glacial reverse-faulting earthquakes of Fennoscandia occurred at a time when the regional horizontal strain rate field was extensional. We argue that this apparent contradiction between extensional horizontal strain rates and reverse faulting earthquakes is an indication that the stable continental lithosphere is able to store long-term tectonic strain and stress, which can be intermittently released in intraplate earthquakes. We discuss the implications of this finding for the earthquake cycle model and for hazard assessment in stable continental regions.

2. Model Construction

Existing three-dimensional models for glacially induced lithospheric deformation range from fully spherical spectral models [e.g., *Wu et al.*, 1999; *Wu and Johnston*, 2000; *Lambeck and Purcell*, 2003], similar in approach to that employed here, to more detailed, but spatially limited to a particular region, flat-Earth finite element models [e.g., *Hampel et al.*, 2009; *Lund et al.*, 2009; *Brandes et al.*, 2015]. Smaller-scale modeling studies have focused on the evolution of slip on discrete faults over a glacial loading cycle [*Hampel and Hetzel*, 2006; *Turpeinen et al.*, 2008; *Hampel et al.*, 2010; *Steffen et al.*, 2014a, 2014b]. While the capacity to accommodate discrete slip on individual faults is not included in our modeling approach, these studies, often conducted in 2-D, do not consider the 3-D response of a coupled crust-whole mantle spherical Earth to glacially induced stresses and strains. In addition, they require a predetermined horizontal strain or stress boundary condition, which, in order to reproduce the observed style of faulting, must be set a priori to be opposite to the observed extension induced by glacial isostatic adjustment.

A common feature of these models is that they all show that the reduction in radial surface stress caused by the removal of the ice load promotes faulting and likely explains the end-glacial clustering for faults located beneath the major ice sheet. Though our own modeling does replicate this finding, our goal is different, as we seek to determine the strain rate field at the time of these end-glacial earthquakes and to compare it with the style of earthquake faulting. Our ultimate motivation is to understand the nature and origin of the strain released by intraplate earthquakes, not the triggering mechanism.

To investigate the relationship between end-glacial faulting in Fennoscandia and the deglaciation-induced stress and strain fields through time, we develop a series of 3-D whole-Earth viscoelastic models exploiting available ice histories across the period of deglaciation. Calculations are performed in three dimensions for a Maxwell viscoelastic self-gravitating Earth (except for in Figures S5 and S6 in the supporting information, where the effect of a Burgers rheology is tested), using the approach of *Cathles* [1975] to calculate an initial elastic response and converting this to a viscoelastic response via the correspondence principle. Our approach calculates the response of a viscoelastic sphere subjected to a periodic surface load, expressed in spherical harmonic coefficients up to degree 128 (corresponding to a wavelength of ~ 300 km at the surface). Boundary conditions are specified at the free surface and at the core-mantle boundary. No far-field tectonic stress field is incorporated into the model and as such is considered to be invariant over the timescale of the model and to be supported within the lithosphere and not subject to any viscous dissipation on the timescale of our models.

Applied surface loading is implemented as predetermined radial stresses at the free surface, based on either the ANU-ICE model developed at the Australian National University, and shown in Figure 1b, or the ICE-5G model [*Peltier*, 2004], shown in Figure S1. Both models are global in extent, and hence, our study on Fennoscandia also incorporates the distal effects of glaciation in North America and Antarctica. Both models are modified to incorporate the effect of changes in oceanic loading, simply by conserving the total water-equivalent load at all time steps and redistributing the removed ice load across the oceans. The computationally-complex full sea level equation is not solved here as it would result in only minor variations of the applied load and hence a negligible change in the predicted stresses and strains in Fennoscandia.

Spherically symmetric, depth-dependent elastic parameters are taken from the seismologically constrained PREM model [*Dziewonski et al.*, 1981]. The model used for the viscosity structure of the Earth depends on the ice loading model used. That used in conjunction with the ANU-ICE model is the model of *Zhao et al.* [2012] (hereafter named ZLL), which comprises an elastic lithosphere over an upper mantle layer and a single lower mantle layer, and is specifically designed to fit geodetic and geological indicators for glacial isostatic adjustment in Fennoscandia. That used in conjunction with the ICE-5G model is the VM5a model of *Peltier and Drummond* [2008], calculated on the basis of fitting present-day geodetic observation of Glacial Isostatic Adjustment in North America. This model comprises an elastic upper lithosphere, a high-viscosity lower

lithosphere, an upper mantle, and two lower mantle layers. Ice and viscosity models are typically derived in tandem, to fit available geological uplift data in rebounding areas (e.g., shoreline displacement and tilting), ice extent indicators through time (e.g., moraines and eskers), and global eustatic sea-level constraints. In the case of both viscosity models used here, regional geodetic data for instrumentally observable uplift rates at the present day was also employed in their derivation (see *Peltier and Drummond* [2008] and *Zhao et al.* [2012] for comparison between modeled displacements and data). Both models are capable of appropriately reproducing available observational data, and the differences between them do not affect our conclusions (see supporting information for a comparison between models and Figure S2 for a comparison with observational geodetic data in Fennoscandia).

For the ANU-ICE model, which covers multiple glacial cycles back to 250 ka, linear interpolation is used to extrapolate the model to a uniform 1 kyr time spacing. Deglaciation is then assumed to be followed by a further 250 kyrs of zero load change. In the case of ICE-5G, the available versions of which do not detail the progression of glaciation up to the point of peak loading, initial loading is assumed to be linear over 75 kyrs, stable for 5 kyrs, and then deglaciation is followed by 200 kyrs of zero load change. In both cases, the end of the zero load change phase is then merged back into the start of the loading cycle to form a period load cycle. The importance of the time step used was tested by linearly interpolating both models to smaller time steps (500 and 250 years), and this was found to make only minimal difference to the broad-scale model outputs, resulting largely due to variations in the onset of the viscous part of the response. Models were also tested for their sensitivity to the values used for the thicknesses of the elastic layer and the viscosities used for the underlying viscous layers (see Figures S5 and S6). In line with the conclusions of *Wu et al.* [1999], these effects are found to be minimal when variations are confined to the range of values consistent with geological data.

The results shown in Figures 2 and 3 (and in Figures S5 and S7) uses the ANU-ICE loading model shown in Figure 1b and linked viscosity model tailored for Fennoscandia [*Zhao et al.*, 2012]. Similar calculations, instead of using the alternative ICE-5G loading model (shown in Figure S1) and the linked VM5a viscosity model [*Peltier and Drummond*, 2008], are included in the supporting information (Figures S3, S4, S6, and S8) and yield similar results to those discussed here. The principle difference is in the rate of ice removal, which is more gradual in ANU-ICE, and focused into two main periods in ICE-5G, leading to a more temporally distributed deformation signal in the ANU-ICE models.

The values shown in all figures except Figure S2 are calculated at a depth of 10 km below the free surface, consistent with the thickness of the seismogenic crust in Fennoscandia, which extends to 30–35 km [*Lindblom et al.*, 2015]. Rates of displacement, strain, and stress are calculated by differencing the spherical harmonic coefficient expression of the deformation at adjacent time steps prior to the calculation of spatial differentials. Rates of change in the stress state on faults are determined from the full stress tensor and differenced after resolving onto the fault.

This model does not include the potential for ice dynamics to influence the crustal pore pressure. However, while the potential for surface transients in pore fluid to penetrate to the depths of earthquake nucleation remains largely unknown, this would operate in a similar manner to the changes in surface stress [*Johnston*, 1987], with ice sheets likely inhibiting meteoric water penetration during glaciation. Deglaciation would then be followed by a renewal of meteoric water, potential reduction of the effective normal stress, and potential earthquake triggering. Unmodeled pore fluid pressure changes could therefore affect the magnitude of normal stress shown in Figures 2 and 3 and could significantly alter the Coulomb stress change calculation shown in Figure 3. Pore fluid changes would not, however, substantially affect the glacially induced strain field.

3. Results

Figures 2 and 3 summarize the model results around the time of activity of the end-glacial faults of Fennoscandia for the ANU-ICE (ZLL) model. Figures 2a–2d shows the evolution of the induced strain rate field from 12 ka to 8 ka across Fennoscandia, along with the rates of change in the normal stress (Figure 2e–h) on a hypothetical fault orientated with the general trend of end glacial faults shown on Figure 1b (strike = 035°, dip = 40°). Figure 3 then focuses in on the peak in the modeled strain rates, at 11–10 ka, showing calculations for the stressing rates and for the change in the Coulomb failure criterion, for a hypothetical pure reverse fault with the geometry of our generalized end-glacial fault. Equivalent figures for the ICE-5G (VM5a) model are included in the supporting information (Figures S3 and S4) and demonstrate that the principal strain rate and stressing rate patterns are the same for both models, although the magnitudes may differ by up to a factor of 2.

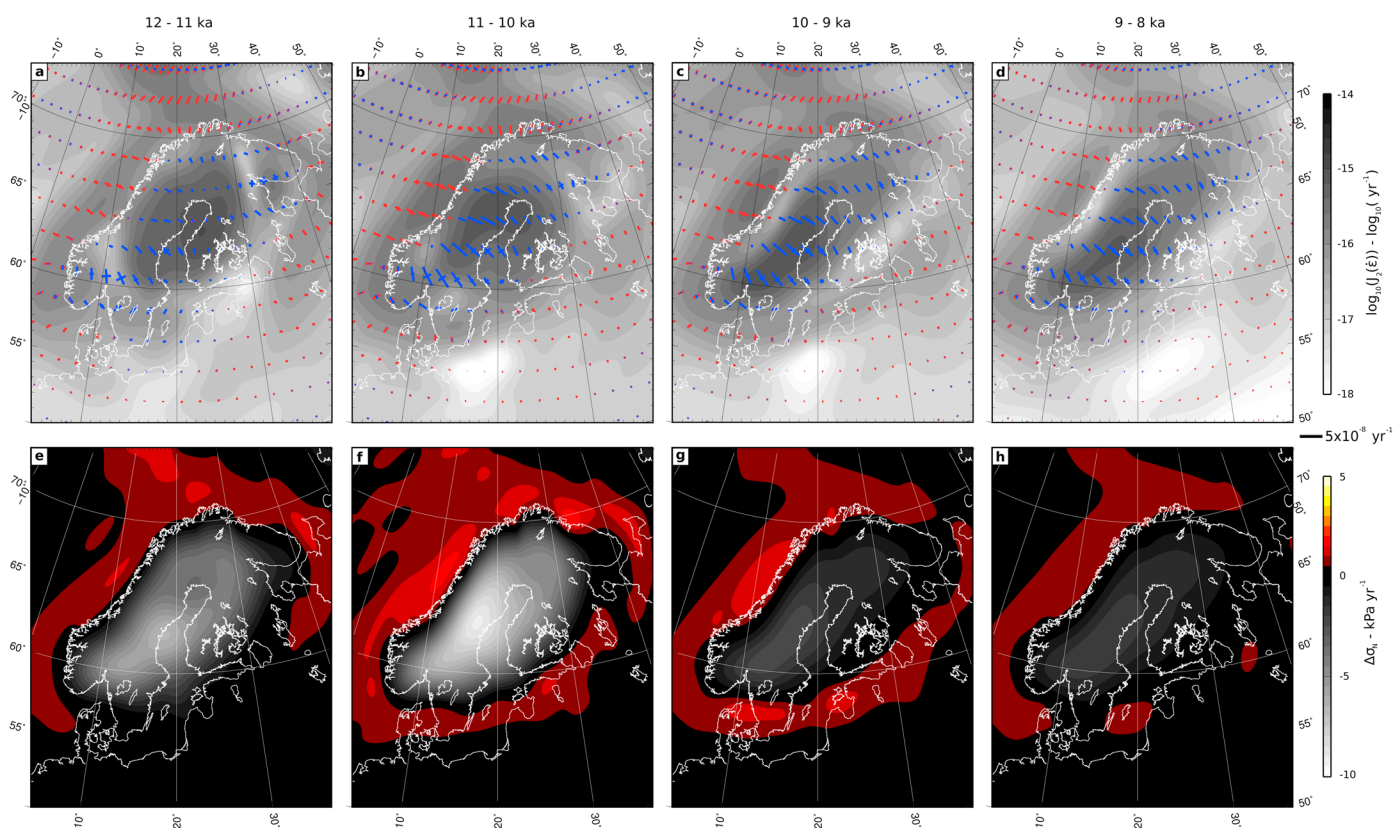


Figure 2. Model results from 12 to 8 ka for the ANU-ICE (ZLL) model. Calculated with a 1 kyr time resolution. (a–d) Second invariant of the deviatoric strain rate tensor, overlain by the principal axes of the horizontal strain rate tensor (colored blue for extension and red for compression). (e–h) Rate of change of applied normal stress on a fault representative of the overall trend of the majority of known major end-glacial faults (strike = 035°, and dip = 40°). Time intervals for each column pair are indicated above.

The similarity between Figures 2 and 3, and Figures S3 and S4 gives us confidence that the conclusions we shall draw below are independent on the finer details of the ice model used.

As Figure 2 demonstrates, the deglaciation-induced strain rate field across Fennoscandia at the time of the end-glacial reverse faulting earthquakes is dominated by NW-SE extension, roughly perpendicular to the general strike of end-glacial faults, and in an overall pattern similar to, although substantially more rapid than, the present (Figure 3a). The peak in strain rate, and in the rate of change in fault-normal stress, coincides within one time step of the peak in seismicity and also demonstrates that our interpretation of the strain rate field is robust to within a time sensitivity greater than the probable resolution of the ice model (a more detailed assessment of the temporal evolution is given in Figures S7 and S8). Figure 2 also demonstrates that the peak in stressing rate is coupled to a peak in the strain rate, and hence, our conclusions relating to the strain rate field and its relationship to motion on the end-glacial faults are insensitive to the precise temporal resolution of the ice models, as the seismicity can be tied to the stress rate peak, which is also linked to a spike in the extensional strain rate field).

Similarly, if we consider the cumulative stresses accrued over a glacial cycle on a fault in the typical orientation of the end-glacial faults, relative to the fully relaxed state (Figure 4), we see that the period at around 11–10 ka not only corresponds to a peak in the rate of increase in the Coulomb failure stress but also leads to the overall peak in cumulative Coulomb stress on our generalized end-glacial fault, which then decays away rapidly to the present. This peak during the final stages of deglaciation is in fact the first time since the onset of this phase of glaciation that we predict a positive Coulomb failure stress due to the influence of the glacial process.

With a dominantly NW-SE extensional strain rate field spanning the time period of major activity on the end-glacial faults of Fennoscandia, it appears that the strain released by these end-glacial earthquakes is opposite to the horizontal strain accumulating at the time of failure, a counter-intuitive result that combines two elements.

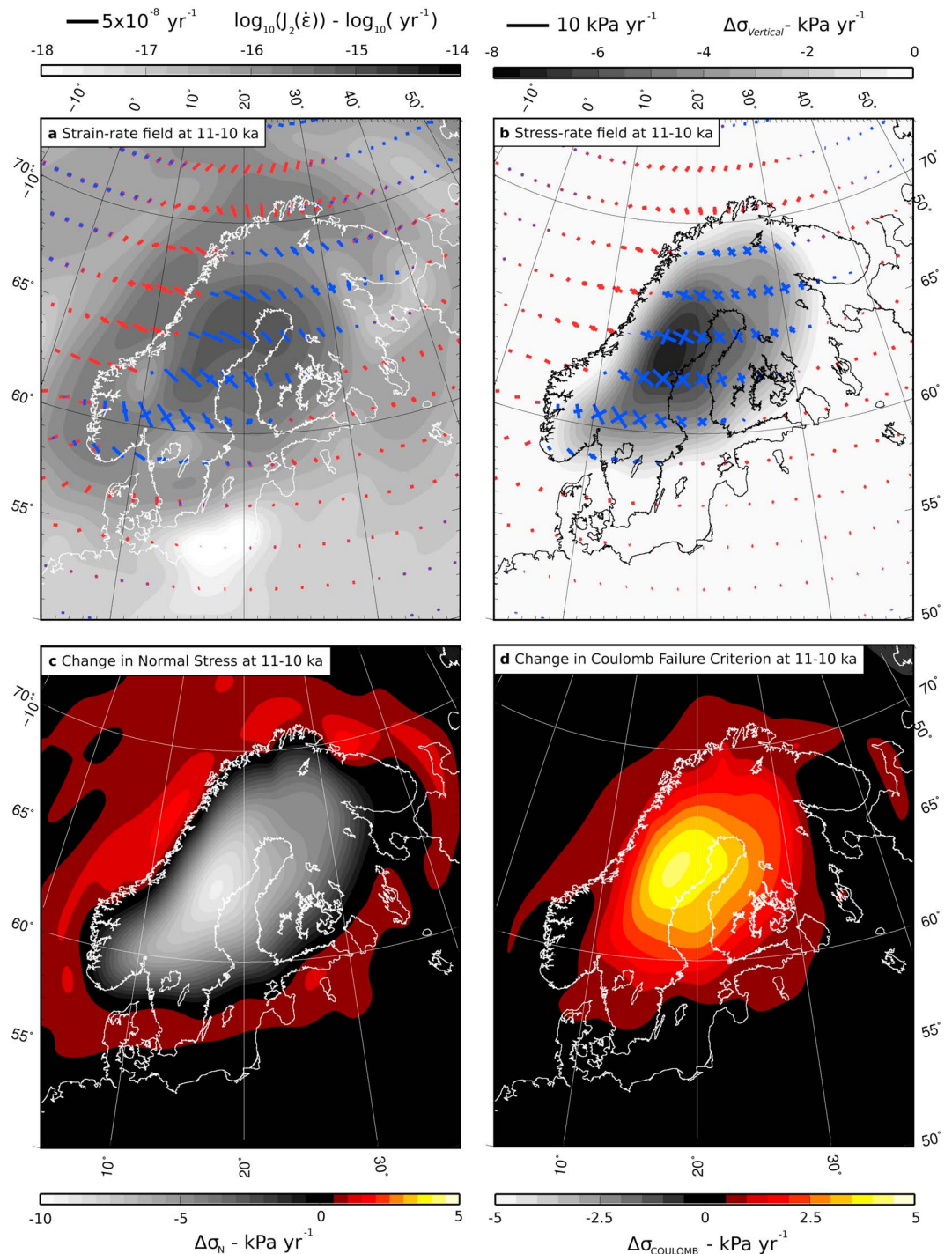


Figure 3. Model results for the ANU-ICE (ZLL) model, calculated for the time interval from 11 to 10 ka. (a) Second invariant of the deviatoric strain rate tensor, overlain by the principle axes of the horizontal strain rate tensor (colored blue for extension and red for compression). (b) The principal axes of the stressing rate tensor. Shading indicates the magnitude of the near-vertical axis, and crosses represent the near-horizontal axes (blue indicates a decrease and red an increase). (c) Rate of change of applied normal stress on a fault representative of the overall trend of the majority of known major end-glacial faults (strike = 035°, and dip = 40°). (d) Change in the Coulomb failure criterion on a similarly orientated fault, assuming preexisting shear stresses are consistent with pure thrust motion on the fault and an effective coefficient of friction of 0.4.

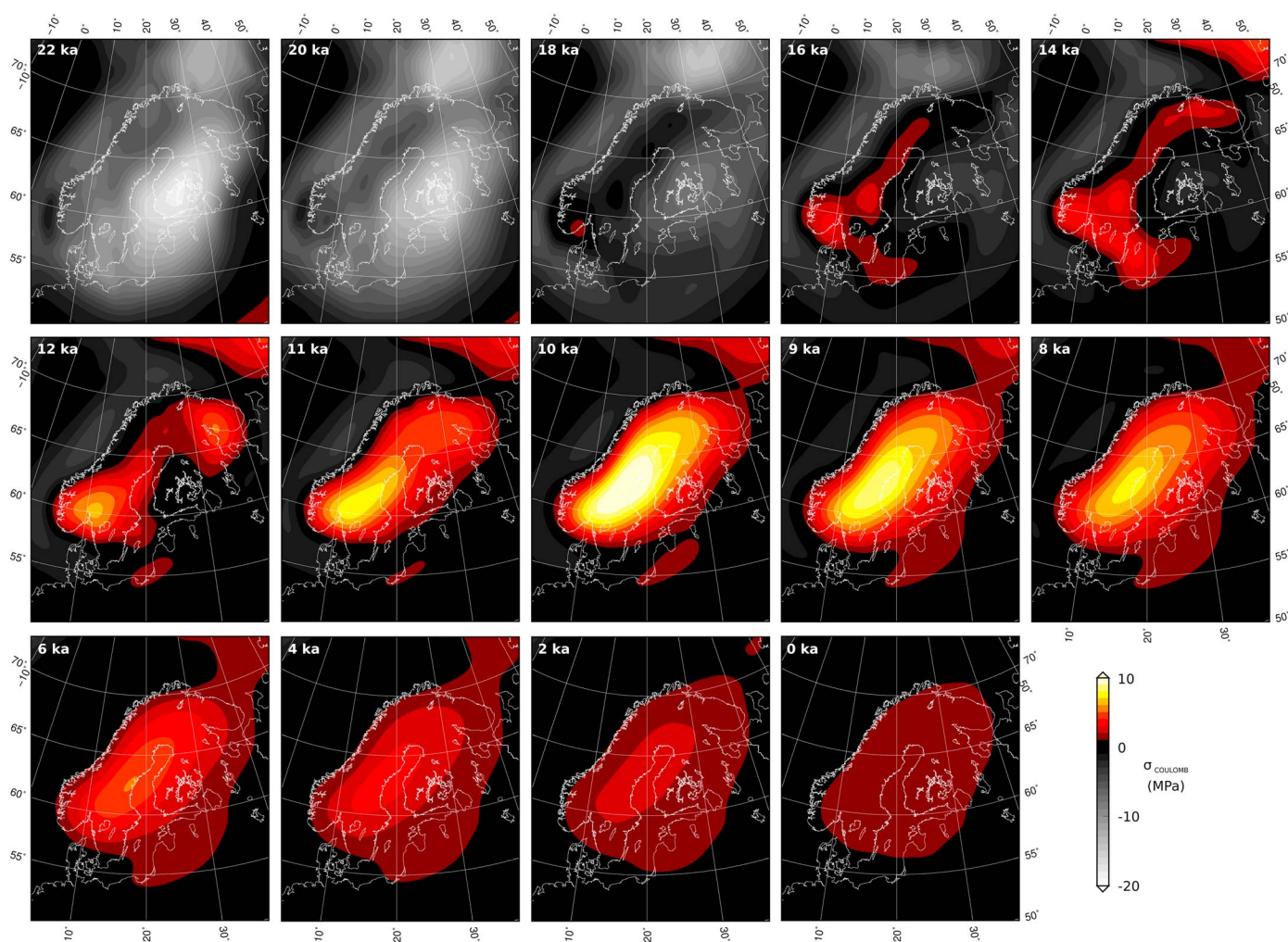


Figure 4. Cumulative Coulomb failure stresses due to glacial loading on a fault representative of the overall trend of the majority of known major end-glacial faults (strike = 035° , and dip = 40°), assuming preexisting shear stresses are consistent with pure thrust motion on the fault and an effective coefficient of friction of 0.4. The time of each panel is indicated in the top right corner. No tectonic loading rates, or overall tectonic stresses, are included.

First, consistent with previous studies [Wu *et al.*, 1999; Lambeck and Purcell, 2003; Hampel *et al.*, 2009; Lund *et al.*, 2009], we find that the removal of the ice load, and hence the reduction in vertical stress at the surface, reduces the normal stress on NNE-SSW-striking thrust faults (Figures 2e–2h). This “unclamping” decreases the shear stress required to cause failure, hence triggering rupture on faults where the shear stress was already close to that required for failure. The rates of change in normal stress are geologically rapid ($1 - 10 \text{ kPa yr}^{-1}$) and hence explain the temporally clustered nature of this end-glacial seismicity. Calculations for the Coulomb failure criterion, although heavily dependent on largely unconstrained factors such as the coefficient of friction and the slip vector of motion on the fault, support this conclusion, with a significant increase in the failure criterion for a pure reverse fault indicated (Figure 3d), leading to the first positive Coulomb failure stress due to the cumulative effect of glacially driven deformation on end-glacial thrust faults since the onset of glaciation (Figure 4).

Second, while the instantaneous horizontal strain and stressing rate is dominantly NW-SE extensional (see Figure 3b), this would only result in a slight decrease in the long-term horizontal compressional stress, due to either the tectonic stress field [Heironymus *et al.*, 2008; Pascal *et al.*, 2010] or the cumulative effect of glacial loading over the glacial cycle. The instantaneous deglaciation-induced stressing rates at the time of failure are therefore acting to lower the magnitude of the background horizontal stress, which still remains compressional overall. Faults rupturing as a result of the rapid decrease in vertical stress therefore have a reverse sense of motion, governed by the background compressional stress state. At the same time, the combination of the

large and transient, glacially induced tensional stressing rates with any background compressional tectonic stressing rate result in an extensional strain rate field that remains measurable until today.

While the cumulative stress and strain induced by glacial loading are typically compressional on both horizontal axes for regions beneath the ice sheet, the role that background tectonic stress plays in end-glacial faulting is ably demonstrated by the dominant orientation of end-glacial fault scarps. The majority, from Finnish Lapland down to southern Sweden, strike along a consistent NNE-SSW trend [Lagerbäck and Sundh, 2008], while the Scandinavian shield is cut by relict faults in a range of orientations, and the load itself (and hence the stress it induced) is more radially symmetric than linear. Such a consistent alignment in fault orientation is therefore not compatible with the failure of faults solely loaded by glacially induced stresses but requires the dominant fault orientation (and the overall stress field) to be governed by the more unidirectional tectonically derived stresses, in the case of Fennoscandia, dominated by the effects of ridge push from the Mid-Atlantic and Gakkel Ridges to the west and north [Heironymus *et al.*, 2008].

Following the removal of the major ice load, and the end of the unclamping triggering mechanism, the ongoing glacially induced strain rate field acts counter to the orientation of both the cumulative glacially driven strain and the tectonically driven field in central Fennoscandia, resulting in the ongoing reduction of the overall compressive stress and strain and likely contributing to the relatively low rates of seismicity in present day Fennoscandia relative to the geodetically observed rates of deformation [Keiding *et al.*, 2015] and increasing the contrast to the pulse of seismicity at 11–9 ka. Additionally, the pulse at 11–9 ka further stands out against the background seismicity rate, due to the predicted inhibition of sub-ice sheet seismicity on faults similar to the observed end-glacial fault during the loading and initial unloading phase [Johnston, 1987], as predicted from the negative cumulative Coulomb failure stresses predicted prior to midglaciation (Figure 4) [see also Lund *et al.*, 2009]. The effects of any ongoing tectonic deformation during the glacial cycle would therefore have been delayed until this point.

Figures S7 and S8 summarize the temporal evolution over the whole deglaciation cycle at the location of four of the principal end-glacial for the two ice models and demonstrate that our model appropriately explains the marked peak in seismic activity focused around 11–9 ka, coincident with major peaks in the horizontal extensional strain rate and rates of change of normal and Coulomb stresses on the faults. A significant decrease in the normal stress on faults with geometries similar to those seen in Fennoscandian fault scarps at this time leads to a rapid increase in the predicted Coulomb failure stress for thrust faults and a maximum in the cumulative Coulomb failure stress over the full glacial cycle, resulting in fault rupture. In each case, this is accompanied by extensional horizontal strain rates. In the case of ICE-5G (Figures S8 and S9), this peak is highly focused due to a rapid phase of ice removal at 10 ka, the resultant reduction in radial stress at the surface, and the instantaneous elastic response. In ANU-ICE, ice removal is more gradual (see Figures 1 and S1), leading to a more distributed signal but still with a peak focused around 10 ka (Figures 4 and S7).

It is notable that our models also predict relatively large stressing rates at times prior to the established peak in seismicity at 11–9 ka, especially for orientations different to that evidenced by known end-glacial faults. While we know of no paleoseismic evidence for major seismicity in Fennoscandia during the rest of the deglaciation period prior to final termination, we note that observational evidence cannot reliably confirm or exclude the existence of major earthquakes during this period, due to the probable removal of any geomorphic expression from subglacial earthquakes that did occur while substantial ice thicknesses were still present.

4. Discussion

The occurrence of end-glacial reverse faulting earthquakes in Fennoscandia in an environment where the large-scale contemporaneous horizontal strain rate was dominated by rapid extension (up to 10^{-7} yr⁻¹) implies that these events did not release the strain that was building up at the time as a result of deglaciation. Therefore, these earthquakes must have released compressional strain that accumulated through long-term tectonic forcing and was stored in the lithosphere, although the last glacial loading stage could have induced a fraction of this strain as well. This has two important implications for our understanding of earthquakes in intraplate settings and the seismic hazard they pose.

First, the temporal clustering of these end-glacial earthquakes highlights the role that geologically rapid non-tectonic changes in stress can play in triggering and localizing seismicity in prestressed continental interiors. Although the influence of glacial loading is unlikely to affect regions much beyond the boundaries of major

ice sheets, other sources of geologically rapid stress changes such as erosion and deposition [Calais *et al.*, 2010; Vernant *et al.*, 2010; Steer *et al.*, 2014] and fluid injection [Keranen *et al.*, 2013; Ellsworth *et al.*, 2015] are also capable of triggering large earthquakes. With decadal-scale fluctuations in the rates of small-scale seismicity in the Gulf of Alaska already correlated to rates of terrestrial ice mass wastage [Sauber and Molnia, 2004; Sauber and Ruppert, 2008], the potential for major deglaciation of the Greenland and Antarctic ice sheets to trigger future large-scale seismic activity [e.g., Johnston, 1987] not accurately characterized by their negligible instrumentally recorded seismicity, or by their present-day strain rate fields, is of particular interest. Other potential localized triggers, such as varying sea level and sediment redistribution, are also possible [Luttrell and Sandwell, 2010; Brothers *et al.*, 2011, 2013], although the magnitudes of strain and stress transients will be much smaller than in the example explored here.

Second, the capacity for geologically short-term variations in surface processes to impact upon the seismogenic behavior of plate interiors implies that the low—often undetectable—strain rates in such regions are not necessarily representative of their earthquake potential, the mode of failure in possible earthquakes, or the regional seismic hazard. That earthquakes in plate interiors release tectonic strain and stress stored over long geological time intervals implies that rupture in such a context can occur on any pre-stressed fault that is favourably oriented in the regional tectonic stress field, provided that local stress changes caused by surface or subsurface processes act to promote failure. This is observed on a daily basis, though with magnitudes that do not exceed M_w 5.7 so far, in regions where wastewater injection into bedrock triggers human-induced seismicity, such as in the southcentral U.S. currently [Keranen *et al.*, 2013; Ellsworth *et al.*, 2015]. In cases where the tectonic stressing rates are significantly higher than any external forcing (as is typically the case at plate boundaries), the external forcing may have only a minor modulating effect on the seismic cycle. In cases where the external forcing rates are significantly greater than the background tectonics, this external forcing may dominate the localization of activity in space and time.

Once an earthquake has released the available stresses on a fault segment, the low background tectonic stressing rate in plate interiors will likely be insufficient to bring it back to the point of failure on an observable timescale. As a consequence, faults may appear to fail only once, as observed for a number of ruptures in stable continental interiors [Crone *et al.*, 2003]. Therefore, seismicity in such a context may be predominantly a transient feature triggered or inhibited by secondary nontectonic sources of stress change rather than a steady state response of faults to a quasi-constant tectonic stress field. Given that long-term elastic strain appears to be available within the lithosphere, as shown here in Fennoscandia, and that faults in stable continental interiors are clearly sensitive to external forcing processes and most in a state of failure equilibrium [e.g., Zoback and Healy, 1992; Townend and Zoback, 2000], it follows that their seismic potential is likely to be more spatially distributed than indicated by paleoearthquakes, current seismicity, or geodetic strain rates. A better understanding of the role that such nontectonic processes may play, and their spatial evolution through time is therefore required for a more complete understanding of the risk posed by rare earthquakes in continental interiors.

5. Conclusion

We have shown that a period of major seismic activity in Fennoscandia, coincident with the final phase of regional deglaciation, occurred as the contemporaneous horizontal strain rate was extensional, opposite to the reverse sense of coseismic displacement on these faults. Therefore, failure on these end-glacial faults did not release extensional elastic strain that was building up at the time of failure but compressional elastic strain that had accumulated in the lithosphere on timescales similar to, or longer than, the glacial cycle. Hence, the tectonically stable continental lithosphere can store elastic strain on long timescales, the release of which may be triggered by rapid, local, and transient stress changes caused by erosion, fluid migration, or ice loading, resulting in the intermittent occurrence of intraplate seismicity, where tectonic loading rates are low relative to shorter-term transients.

That earthquakes in plate interiors release long-term tectonic strain implies that rupture in such a context can occur on any prestressed fault favourably oriented with the regional tectonic stress field. Seismic hazard in such settings is therefore heavily dependent on localized transient stress changes of nontectonic origin tapping into the background tectonic stress field and is likely to be more spatially distributed than indicated by paleoearthquakes, current seismicity, or geodetic strain rates.

Acknowledgments

We thank the Editor, Andrew Newman, and two anonymous reviewers for their careful comments which helped improve the manuscript. This work was funded through the French Investment Program SINAPS project through the Commissariat à l'Énergie Atomique (CEA/DASE/LDG) and the Institut de Radioprotection et Sûreté Nucléaire (IRSN). The work was hosted at the Yves Rocard Joint Laboratory (ENS, CNRS, and CEA/DASE). We are grateful to the Geological Survey of Sweden for providing detailed information on known fault scarps in Sweden. We thank Kurt Lambeck and Hélène Rouby for making the compiled ANU-ICE model available.

References

- Arvidsson, R. (1996), Fennoscandian earthquakes: Whole crustal rupturing related to postglacial rebound, *Science*, *274*, 744–746.
- Brandes, C., H. Steffen, R. Steffen, and P. Wu (2015), Intraplate seismicity in northern Central Europe is induced by the last glaciation, *Geology*, *43*, 611–614, doi:10.1130/G36710.1.
- Brothers, D., D. Kilb, K. Luttrell, N. Driscoll, and G. Kent (2011), Loading of the San Andreas fault by flood-induced rupture of faults beneath the Salton Sea, *Nat. Geosci.*, *4*(7), 486–492.
- Brothers, D. S., K. M. Luttrell, and J. D. Chaytor (2013), Sea-level-induced seismicity and submarine landslide occurrence, *Geology*, *41*(9), 979–982.
- Calais, E., and S. Stein (2009), Time-variable deformation in the New Madrid seismic zone, *Science*, *323*, 1442, doi:10.1126/science.1168122.
- Calais, E., A. M. Freed, R. Van Arsdale, and S. Stein (2010), Triggering of New Madrid Seismicity by late-Pleistocene erosion, *Nature*, *466*, 608–611, doi:10.1038/nature09258.
- Cathles, L. (1975), *Viscosity of the Earth's Mantle*, Princeton Univ. Press, Princeton, N. J.
- Craig, T. J., and E. Calais (2014), Strain accumulation in the New Madrid and Wabash Valley Seismic Zones from 14 years of continuous GPS observation, *J. Geophys. Res. Solid Earth*, *119*, 9110–9129, doi:10.1002/2014JB011498.
- Crone, A. J., and K. V. Luza (1990), Style and timing of Holocene surface faulting on the Meers fault, southwestern Oklahoma, *Geol. Soc. Am. Bull.*, *102*, 1–17.
- Crone, A. J., P. M. De Martini, M. N. Machette, K. Okumura, and J. R. Prescott (2003), Paleoseismicity of two historically quiescent faults in Australia: Implications for fault behavior in stable continental regions, *Bull. Seismol. Soc. Am.*, *93*(5), 1913–1934.
- Dziewonski, A. M., T.-A. Chou, and J. H. Woodhouse (1981), Determination of earthquake source parameters from waveform data for studies of global and regional seismicity, *J. Geophys. Res.*, *86*, 2825–2852.
- Ellsworth, W. L., A. L. Llenos, A. F. McGarr, A. J. Michale, J. L. Rubenstein, C. S. Mueller, M. D. Petersen, and E. Calais (2015), Increasing seismicity in the U.S. midcontinent: Implications for earthquake hazard, *Leading Edge*, *34*, 618–626.
- England, P., and J. Jackson (2012), Uncharted seismic risk, *Nat. Geosci.*, *4*, 248–249.
- Hampel, A., and R. Hetzel (2006), Response of normal faults to glacial-interglacial fluctuations of ice and water masses on Earth's surface, *J. Geophys. Res.*, *111*, B06406, doi:10.1029/2005JB004124.
- Hampel, A., R. Hetzel, G. Maniatis, and T. Karow (2009), Three-dimensional numerical modeling of slip rate variations on normal and thrust fault arrays during ice cap growth and melting, *J. Geophys. Res.*, *114*, B08406, doi:10.1029/2008JB006113.
- Hampel, A., T. Karow, G. Maniatis, and R. Hetzel (2010), Slip rate variation on faults during glacial loading and post-glacial unloading: Implications for the viscosity structure of the lithosphere, *J. Geol. Soc. London*, *167*, 385–399, doi:10.1144/0016-76492008-137.
- Heironymus, C. F., S. Goes, M. Sargent, and G. Morra (2008), A dynamical model for generating Eurasian lithospheric stress and strain rate fields: Effect of rheology and cratons, *J. Geophys. Res.*, *113*, B07404, doi:10.1029/2007JB004953.
- Hough, S. E., and M. Page (2011), Toward a consistent model for strain accrual and release for the New Madrid Seismic Zone, central United States, *J. Geophys. Res.*, *116*, B03311, doi:10.1029/2010JB007783.
- Jakobsen, M., S. Björck, M. O'Regan, T. Flodén, S. L. Greenwood, H. Swärd, A. Lif, L. Ampel, H. Koyi, and A. Skelton (2014), Major earthquake at the Pleistocene-Holocene transition in Lake Vättern, southern Sweden, *Geology*, *42*, 379–382, doi:10.1130/G35499.1.
- Johnston, A. C. (1987), Suppression of earthquakes by large continental ice sheets, *Nature*, *330*, 467–469.
- Juhlin, C., M. Dehghannejad, B. Lund, A. Malehmir, and G. Pratt (2010), Reflection seismic imaging of the end-glacial Pärvie Fault system, northern Sweden, *J. Appl. Geophys.*, *70*, 307–316, doi:10.1016/j.jappgeo.2009.06.004.
- Keiding, M., C. Kreemer, C. D. Lindholm, S. Gradmann, O. Olesen, and H. P. Keirulf (2015), A comparison of strain rates and seismicity for Fennoscandia: Depth dependency of deformation from glacial isostatic adjustment, *Geophys. J. Int.*, *202*, 1021–1028, doi:10.1093/gji/ggv207.
- Kenner, S. J., and P. Segall (2000), A mechanical model for intraplate earthquakes: Application to the New Madrid seismic zone, *Science*, *289*, 2329–2332.
- Keranen, K. M., H. M. Savage, G. A. Abers, and E. S. Cochran (2013), Potentially induced earthquakes in Oklahoma, USA: Links between wastewater injection and the 2011 Mw 5.7 earthquake sequence, *Geology*, *41*, 699–702.
- Kierulf, H. P., H. Steffen, M. J. R. Simpson, M. Lidberg, P. Wu, and H. Wang (2014), A GPS velocity field for Fennoscandia and a consistent comparison to glacial isostatic adjustment models, *J. Geophys. Res. Solid Earth*, *119*, 6613–6629, doi:10.1002/2013JB010889.
- Kotilainen, A., and K.-L. Hutri (2004), Submarine Holocene sedimentary disturbances in the Olkio area of the Gulf of Bothnia, Baltic Sea: A case of postglacial paleoseismicity, *Quat. Sci. Rev.*, *23*, 1125–1135, doi:10.1016/j.quascirev.2003.12.002.
- Lagerbäck, R. (1978), Neotectonic structure in northern Sweden, *Geol. Foeren. Stockholm Foerh.*, *100*, 263–269, doi:10.1080/11035897809452533.
- Lagerbäck, R., and M. Sundh (2008), *Early Holocene Faulting and Paleoseismicity in Northern Sweden*, Res. Pap. C, vol. 836, Sveriges geologiska undersökning, Uppsala, Sweden.
- Lambeck, K., and A. Purcell (2003), Glacial rebound and crustal stress in Finland, Tech. Rep. 2003-10, Posiva, Finland.
- Lindblom, E., B. Lund, A. Tryggvason, M. Uski, R. Bödvarsson, C. Juhlin, and R. Roberts (2015), Microearthquakes illuminate the deep structure of the endglacial Pärvie fault, northern Sweden, *Geophys. J. Int.*, *201*, 1704–1716, doi:10.1093/gji/ggv112.
- Lindholm, C. D., H. Bungum, E. Hicks, and M. Villagran (2000), Crustal stress and tectonics in Norwegian regions determined from earthquake focal mechanisms, in *Dynamics of the Norwegian Margin*, edited by A. Nottvedt, *Geol. Soc. London, Spec. Publ.*, *167*, 429–439.
- Liu, M., S. Stein, and H. Wang (2010), 2000 years of migrating earthquakes in North China: How earthquakes in midcontinents differ from those at plate boundaries, *Lithosphere*, *3*, 128–132, doi:10.1130/L129.1.
- Lund, B., and M. D. Zoback (1999), Orientation and magnitude of in situ stress to 6.5 km depth in the Baltic Shield, *Int. J. Rock Mech. Min. Sci.*, *36*, 169–190.
- Lund, B., P. Schimdt, and C. Hieronymus (2009), *Stress Evolution and Fault Stability During the Weichselian Glacial Cycle*, Swedish Nucl. Fuel and Waste Manage. Co (SKB), Stockholm, Sweden.
- Luttrell, K., and D. Sandwell (2010), Ocean loading effects on stress at near shore plate boundary fault systems, *J. Geophys. Res.*, *115*, B08411, doi:10.1029/2009JB006541.
- Muir-Wood, R. (1989), Extraordinary deglaciation reverse faulting in northern Fennoscandia, in *Earthquakes at North Atlantic Passive Margins: Neotectonics and Post-Glacial Rebound*, NATO ASI Ser., edited by S. Gregersen and P. W. Basham, pp. 141–174, Springer, Netherlands.
- Newman, A., S. Stein, J. Weber, J. Engeln, A. Mao, and T. Dixon (1999), Slow deformation and lower seismic hazard at the New Madrid seismic zone, *Science*, *284*, 619–621.

- Olesen, O., H. Bungum, J. Dehls, C. Lindholm, C. Pascal, and D. Roberts (2014), Neotectonics, seismicity and contemporary stress fields in Norway—Mechanisms and implications, in *Quaternary Geology of Norway*, vol. 13, edited by L. Olsen, O. Fredin, and O. Olesen, pp. 145–174, Geol. Surv. of Norway Spec. Publ., Trondheim, Norway.
- Page, M. T., and S. E. Hough (2014), The New Madrid seismic zone: Not dead yet, *Science*, *343*, 762–764, doi:10.1126/science.1248215.
- Pascal, C., D. Roberts, and R. H. Gabrielsen (2010), Tectonic significance of present-day stress relief phenomena in formerly glaciated regions, *J. Geol. Soc. London*, *167*, 363–371, doi:10.1144/0016-76492009-136.
- Peltier, W. R. (2004), Global glacial isostasy and the surface of the Ice-Age Earth: The ICE-5G (VM2) model and GRACE, *Annu. Rev. Earth Planet. Sci.*, *32*, 111–149.
- Peltier, W. R., and R. Drummond (2008), Rheological stratification of the lithosphere: A direct inference based upon the geodetically observed pattern of the glacial isostatic adjustment of the North American continent, *Geophys. Res. Lett.*, *35*, L16314, doi:10.1029/2008GL034586.
- Sauber, J., and N. A. Ruppert (2008), Rapid ice mass loss: Does it have an influence on earthquake occurrence in Southern Alaska, in *Active Tectonics and Seismic Potential of Alaska*, *Geophys. Monogr. Ser.*, vol. 179, edited by J. T. Freymueller et al., AGU, Washington, D. C., doi:10.1029/179GM21.
- Sauber, J. M., and B. F. Molnia (2004), Glacier ice mass fluctuations and fault instability in tectonically active southern Alaska, *Global Planet. Change*, *42*, 279–293, doi:10.1016/j.gloplacha.2003.11.012.
- Slunga, R. S. (1991), The Baltic shield earthquakes, *Tectonophysics*, *189*, 323–331.
- Smalley, R., M. A. Ellis, J. Paul, and R. B. Van Arsdale (2005), Space geodetic evidence for rapid strain rates in the New Madrid seismic zone of central USA, *Nature*, *435*, 1088–1090, doi:10.1038/nature03642.
- Smith, C., M. Sundh, and H. Mikko (2014), Surficial geology indicates early Holocene faulting and seismicity, central Sweden, *Int. J. Earth Sci.*, *103*, 1711–1724, doi:10.1007/s00531-014-1025-6.
- Steer, P., M. Simoes, R. Cattin, and J. B. H. Shyu (2014), Erosion influences the seismicity of active thrust faults, *Nat. Commun.*, *5*, 5564, doi:10.1038/ncomms6564.
- Steffen, R., H. Steffen, P. Wu, and D. W. Eaton (2014a), Stress and fault parameters affecting fault slip magnitude and activation time during a glacial cycle, *Tectonics*, *33*, 1461–1476, doi:10.1002/2013TC003450.
- Steffen, R., P. Wu, H. Steffen, and D. W. Eaton (2014b), The effect of earth rheology and ice-sheet size on fault slip and magnitude of postglacial earthquakes, *Earth Planet. Sci. Lett.*, *388*, 71–80, doi:10.1016/j.epsl.2013.11.058.
- Stein, S., and M. Liu (2009), Long aftershock sequences within continents and implications for earthquake hazard assessment, *Nature*, *462*, 87–89, doi:10.1038/nature08502.
- Townend, J., and M. D. Zoback (2000), How faulting keeps the crust strong, *Geology*, *28*(5), 399–402.
- Turpeinen, H., A. Hampel, T. Karow, and G. Maniatis (2008), Effect of ice sheet growth and melting on the slip evolution of thrust faults, *Earth Planet. Sci. Lett.*, *269*, 230–241, doi:10.1016/j.epsl.2008.02.017.
- Vernant, P., H. Hivert, J. Chéry, P. Steer, R. Cattin, and A. Rigo (2010), Erosion-induced isostatic rebound triggers extension in low convergent mountain ranges, *Geology*, *41*, 467–470, doi:10.1130/G33942.1.
- Wu, P., and P. Johnston (2000), Can deglaciation trigger earthquake in N. America?, *Geophys. Res. Lett.*, *27*, 1323–1326.
- Wu, P., P. Johnston, and K. Lambeck (1999), Post-glacial rebound and fault instability in Fennoscandia, *Geophys. J. Int.*, *139*, 657–670, doi:10.1046/j.1365-246x.1999.00963.x.
- Zhao, S., K. Lambeck, and M. Lidberg (2012), Lithosphere thickness and mantle viscosity inverted from GPS-derived deformation rates in Fennoscandia, *Geophys. J. Int.*, *190*, 278–292, doi:10.1111/j.1365-246X.2012.05454.x.
- Zoback, M. D., and J. H. Healy (1992), In situ stress measurements to 3.5 km depth in the Cajon Pass Scientific Research Borehole: Implications for the mechanics of crustal faulting, *J. Geophys. Res.*, *97*, 5039–5057.